

# Graphite–Tin composites as anode materials for lithium-ion batteries

G.X. Wang<sup>a,\*</sup>, Jung-Ho Ahn<sup>b</sup>, M.J. Lindsay<sup>a</sup>, L. Sun<sup>a</sup>,  
D.H. Bradhurst<sup>a</sup>, S.X. Dou<sup>a</sup>, H.K. Liu<sup>a</sup>

<sup>a</sup>*Energy Storage Materials Research Program, Institute for Superconducting and Electronic Materials,  
University of Wollongong, Northfields Avenue, Wollongong NSW 2522, Australia*

<sup>b</sup>*Department of Materials Engineering, Andong National University, Andong, Gyungbulk 760-749, South Korea*

Received 16 June 2000; accepted 31 December 2000

## Abstract

Graphite–tin composites were produced by high-energy ball-milling. X-ray diffraction and HREM observation showed that graphite became amorphous and tin became nanocrystalline after the intensive ball milling. The element Sn was encapsulated in the ductile graphite matrix on a nanometer scale. Electrochemical tests show that the lithium storage capacity increases with the addition of Sn, which could be attributed to the reaction of Sn with Li to form  $\text{Li}_x\text{Sn}$  alloys. The volume expansion due to the alloying process may be buffered by the amorphous graphite matrix. The  $\text{C}_{0.9}\text{Sn}_{0.1}$  electrode can deliver a discharge capacity of 1250 mAh/g in the initial cycle. Generally, the capacity of the ball-milled C,  $\text{C}_{0.9}\text{Sn}_{0.1}$  and  $\text{C}_{0.8}\text{Sn}_{0.2}$  electrodes decrease with cycling quite quickly, but the  $\text{C}_{0.9}\text{Sn}_{0.1}$  and  $\text{C}_{0.8}\text{Sn}_{0.2}$  electrodes have better cyclability than that of the ball-milled graphite electrode. The combination of C and Sn could be an anode material with high capacity for lithium-ion batteries. © 2001 Elsevier Science B.V. All rights reserved.

**Keywords:** Graphite–tin composites; Ball milling; Nanocrystalline; Lithium-ion battery

## 1. Introduction

Lithium-ion batteries are state-of-the-art power sources for portable electronic devices and also show promise for use in electric vehicles (EVs). They have several advantages over traditional rechargeable Ni–Cd and Ni–MH batteries such as no memory effect, high energy density and long cycle life. Carbon materials and  $\text{LiCoO}_2$  or  $\text{LiM}_x\text{Co}_{1-x}\text{O}_2$  compounds are currently used as anode and cathode materials, respectively, in commercial lithium-ion batteries [1–4]. The development of a new generation of lithium-ion batteries demands new cathode and anode materials with higher energy density than that of the existing system. The new high capacity cathode materials may still need some time to develop. By contrast, the capacity of carbon anode materials has been improved greatly in the past few years from early types of soft carbons (200–240 mAh/g) to more recent MCMB graphites (300–340 mAh/g) [5–7]. Some carbonaceous compounds (hard carbon) have demonstrated even higher capacity of about 700 mAh/g [8–12]. In addition to carbon materials, some binary or ternary lithium alloys, intermetallic alloys and tin oxide glass have recently

attracted worldwide attention. In particular, tin was used as the active element, because it can combine with Li to form  $\text{Li}_{22}\text{Sn}_5$  alloys with a theoretical capacity of 990 mAh/g. The main shortcoming for Sn, MSn alloys and tin oxides is the volume expansion during the process of alloying with Li, which causes crumbling and cracking of the electrode, inducing a very short cycle life [13–15]. Dahn et al. [16] have prepared a series of nanocrystalline Fe–Sn intermetallic alloys, which demonstrated high lithium storage capacity and reasonable cyclability.

The objective of this investigation is to combine the high lithium storage capacity of the element Sn and the stable cyclability of graphite. Graphite–tin composites with different content of tin were prepared by high energy ball milling. The physical properties and microstructure of the C–Sn composites were characterized by X-ray diffraction (XRD), TEM and HREM. The electrochemical performance of the composites as anodes was examined using lithium test cells.

## 2. Experimental

The ball-milled graphite and tin powders were produced by high energy ball milling. The mixtures of pure graphite

\* Corresponding author. Fax: +61-2-21-5731.

E-mail address: gw14@uow.edu.au (G.X. Wang).

(1–2  $\mu\text{m}$ , Aldrich) and tin (–325 mesh, 99.8%, Aldrich) with different atomic ratios ( $\text{Sn:C} = 0, 0.1, 0.2$ ) were put into a stainless steel vial. The vial was evacuated and then purged with pure argon. The ball milling was carried out in a planetary ball milling machine (Pulverisette-5, LABTECHNICS, Australia) for 100–120 h at a rotation rate of 300 rpm. The powders produced were characterized by XRD and HREM. XRD was performed using a Philips PW 1730 diffractometer with  $\text{Cu K}\alpha$  radiation. The morphology and microstructure of ball-milled powders were observed by high-resolution electron microscopy, using a EM 2010 (JEOL) high-resolution electron microscope.

CR2032 coin cells were fabricated to test the electrochemical properties of ball-milled C–Sn powders. The C–Sn electrodes were made by dispersing 95 wt.% active materials and 5 wt.% polyvinylidene fluoride (PVDF) binder in dimethyl phthalate solvent to form a slurry, which was then spread on to copper foil. The thickness of the electrode was approximately 60–80  $\mu\text{m}$  with a loading of 1–2 mg. The

cells were assembled in an argon filled glove-box (Mbraun, Unilab, USA), using a hand-operated closing tool (Hosen Co., Japan). The electrolyte was 1 M  $\text{LiPF}_6$  in a mixture of ethylene carbonate (EC) and dimethyl carbonate (DMC) (1:1 by volume, provided by MERCK KGaA, Germany). The cells were galvanostatically charged and discharged in the voltage range of 0–2.5 V versus  $\text{Li}/\text{Li}^+$ .

### 3. Results and discussion

#### 3.1. Structural characterization of C–Sn composites

The typical XRD patterns of ball-milled graphite and graphite–tin composites are shown in Fig. 1(a). For comparison, the XRD pattern of the unmilled graphite is also shown. The unmilled graphite is a well-graphitized 2H graphite with strong (0 0 2) diffraction intensity. After ball milling, the diffraction lines (0 0 2) (1 0 0) and (1 0 1) of graphite

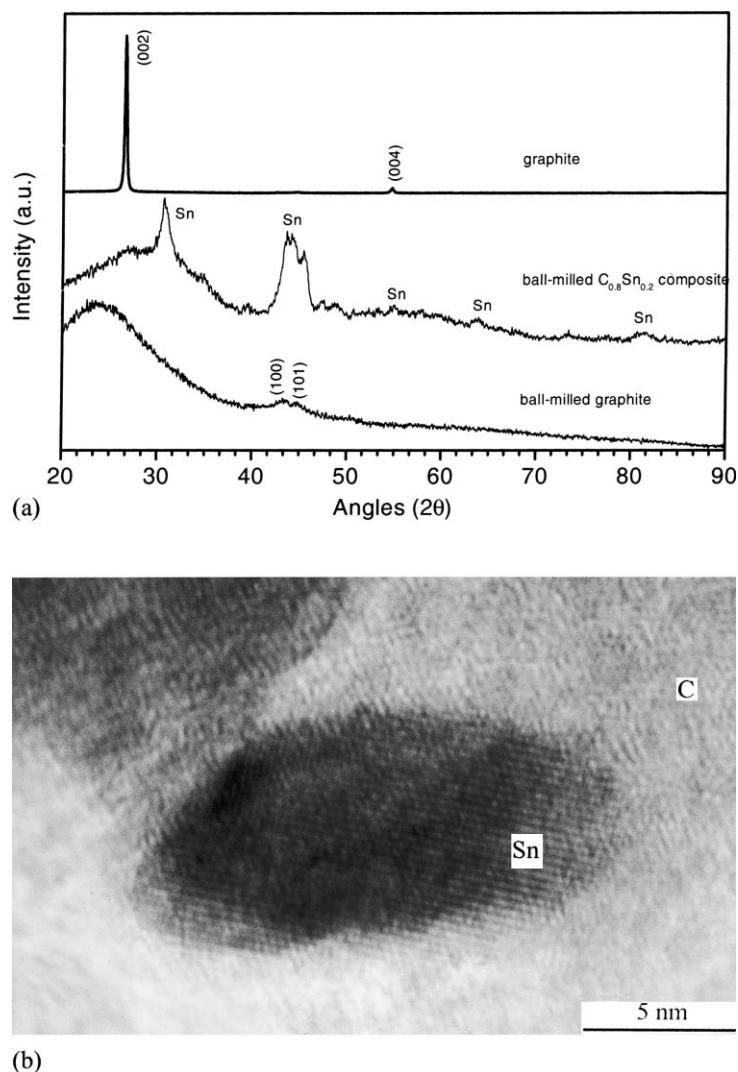


Fig. 1. (a) XRD patterns; (b) HREM image of ball-milled  $\text{C}_{0.8}\text{Sn}_{0.2}$  composite.

became very broad and were shifted to lower angles. The (0 0 4) diffraction line was weak and indistinguishable. The interlayer distances ( $d_{002}$ ) of graphite were 3.355, 3.675, 3.392 and 3.362 Å for unmilled graphite, ball-milled graphite,  $C_{0.8}Sn_{0.2}$  and  $C_{0.9}Sn_{0.1}$ , respectively. In general, the values of  $d_{002}$  for graphite increase after ball milling. The  $d_{002}$  for ball-milled graphite in our investigation is the same as the result found by Shen et al. [17] ( $d_{002} = 3.68$  Å). It has been reported that the increase in  $d_{002}$  by ball milling is attributed to the introduction of interstitial carbon atoms into the initial pristine graphite structure [18]. However, the  $d_{002}$  values in  $C_{0.8}Sn_{0.2}$  and  $C_{0.9}Sn_{0.1}$  composites are much smaller. This might mean that Sn could prevent the interstitial carbon atoms from entering into the pristine graphite structure during ball milling. The degree of diffraction peak broadening for Sn is much smaller than graphite on ball milling. Therefore, it follows that the effect of ball milling on reducing the particle size of tin is less than that on graphite.

The microstructure of ball-milled graphite and graphite–tin composites were observed by HREM. Fig. 1(b) shows the HREM images of ball-milled graphite–tin composite  $C_{0.8}Sn_{0.2}$ . The pristine graphite is a well-organized crystalline structure. After intensive ball milling, graphite became disordered and amorphous. The graphene layers are wrinkled and the interlayer spacings are irregular. Wang et al. [19] proposed that ball-milled graphite consists of many basic structured units (BSU) and the wrinkled layers may be attributed to the interstitial atoms. Microcavities were observed on the edge of BSU. After ball milling, the Sn particles are broken down to 15–20 nm, but still attain an ordered crystalline state, nanocrystalline Sn particles are embedded in a disordered or amorphous carbon matrix. The boundaries between Sn particles and C matrix are very smooth. This demonstrates that there is no obvious gap between Sn particles and the C matrix, which should assist  $Li^+$  ion diffusion and electron transfer between Sn particles and the amorphous graphite matrix.

### 3.2. Electrochemical characteristics of C–Sn composite electrodes

The electrochemical performance of  $C_{1-x}Sn_x$  composites was measured using  $C_{1-x}Sn_x$  as the working electrode and lithium metal as the counter electrode. Fig. 2 shows the discharge/charge profiles for ball-milled graphite and graphite–tin composite electrodes. The first discharge capacity for ball-milled C,  $C_{0.9}Sn_{0.1}$  and  $C_{0.8}Sn_{0.2}$  electrodes were 820, 1250 and 1070 mAh/g, respectively. With the addition of Sn in graphite by ball milling, the specific capacity increased but not in proportion to the Sn content. The  $C_{0.9}Sn_{0.1}$  composite electrode demonstrated the highest capacity. It has been reported that the electrochemical performance of ball-milled C are related to the type of mixer and independent of the morphology and of the state-of-the-starting materials [20]. As indicated from the XRD pattern after ball milling, graphite became disordered and amorphous, in

which there were vacancies, microcavities and a disorganized region. The lithium can be inserted into these vacancies, microcavities, voids or the edges of BSU layers. Most of the reversible capacity is due to lithium storage in these regions [21,22]. However, we observed a large irreversible capacity of 420 mAh/g in the first charge/discharge for ball-milled C electrode. This irreversible capacity, mainly between 1.2 and 0.6 V, is supposed to be caused by the decomposition of the electrolyte and the formation of a passivation film on the surface of the electrode due to the larger surface area of ball-milled graphite. The increased capacities for  $C_{0.8}Sn_{0.2}$  and  $C_{0.9}Sn_{0.1}$  electrodes should be attributed to the nano-dispersed Sn in the graphite matrix, because the ball milling condition was identical for all three samples. It is well known that Sn can react with Li to form  $Li_{4.4}Sn$  alloy.

The differential capacity plots of the first discharge/charge for ball-milled graphite and ball-milled  $C_{0.8}Sn_{0.2}$  electrodes are presented in Fig. 2 as inset. With the scrutiny of these plots, we found that there exist some differences between ball-milled graphite and the  $C_{0.8}Sn_{0.2}$  composite electrodes. In Fig. 1(a), there are two peaks at about 1.4 and 0.1 V, respectively, during the discharge process. The 1.4 V peak also appears in the differential capacity curves of  $C_{0.8}Sn_{0.2}$  electrode during discharge, which is believed to originate from lithium insertion into vacancies in ball-milled graphite, since lithium insertion into vacancies and disorganized regions is at a higher potential than that between interlayers [23]. The differential peaks between 0.5 and 0.6 V during charge and discharge are associated with the alloying reaction between Sn and Li. This means that Sn participated in the reaction. We have tried to prove this mechanism by ex situ XRD. However, we did not identify the Li–Sn alloy phase after C–Sn composite electrodes were discharged. This is probably because Li–Sn alloys formed are in a nanocrystalline or amorphous state. The lithium reaction with Sn to form  $Li_xSn$  alloys can result in a volume increase by 676%, which could induce serious cracking or crumbling of Li–Sn alloy. Any cracking of the Li–Sn alloys will cause the isolation of Sn, increase the impedance and eventually decrease the capacity of the electrode. However, Sn particles were reduced to the nanocrystalline state and dispersed in the graphite matrix after ball milling. Also, the ductile graphite matrix could buffer the expansion of the alloy volume. Therefore, the cyclability of the electrode can be improved. This is shown in Fig. 3. The  $C_{0.8}Sn_{0.2}$  and  $C_{0.9}Sn_{0.1}$  electrodes demonstrated a better rechargeability than that of the ball-milled C electrode. From the previous reports [19,24], ball-milled graphite delivered a large initial lithium insertion capacity, but the capacity degraded with cycling quite quickly. We believe this problem could be solved by optimizing the ball milling conditions to produce carbon materials with appropriate crystal structure and microstructure. Furthermore, adding active Sn to the carbon matrix can improve capacity, and if elementary Sn is dispersed properly, a good cyclability can be achieved.

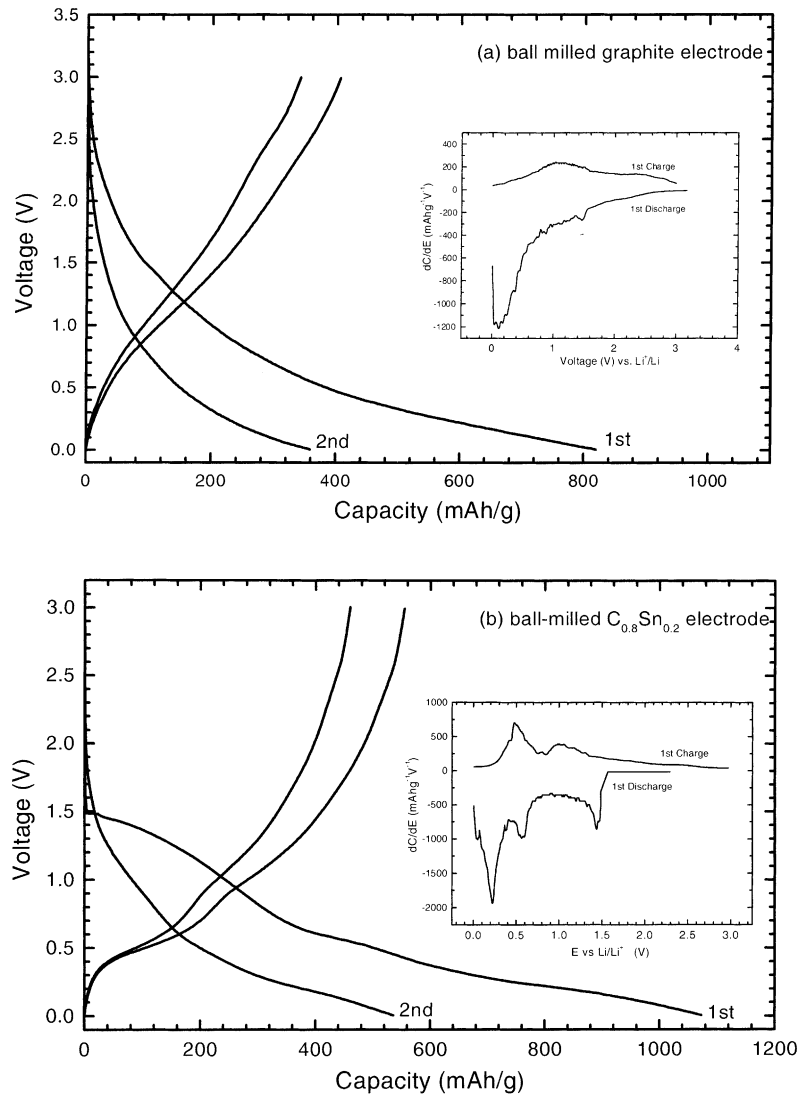


Fig. 2. Discharge and charge curves of ball-milled graphite and graphite–tin composite electrodes. The differential capacity vs. voltage are shown in inset.

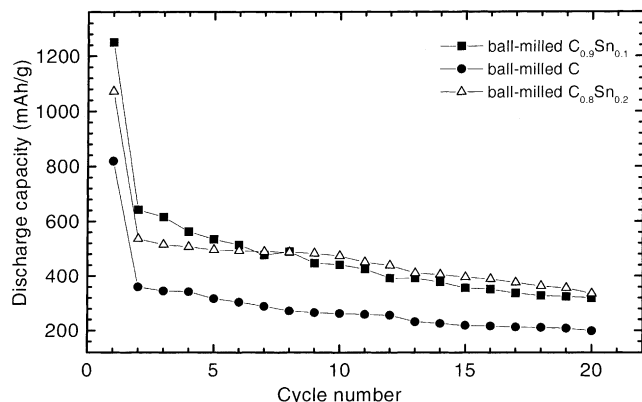


Fig. 3. The discharge capacities vs. cycle number for ball-milled graphite,  $C_{0.8}Sn_{0.2}$  and  $C_{0.9}Sn_{0.1}$  composite electrodes.

#### 4. Conclusions

$C_{1-x}Sn_x$  composites can be prepared by mechanically ball milling raw graphite and tin powders. Graphite was pulverized to a disorganized amorphous state. Sn became nanocrystalline and embedded in the graphite matrix. Electrochemical tests show that  $C_{1-x}Sn_x$  composite electrodes can deliver a large lithium storage capacity of approximately 800–1250 mAh/g, which is two to three times that of graphite. However, a large irreversible capacity after the first cycle prevents their practical application. We believe that optimization of conditions of materials preparation can overcome these disadvantages. Therefore, graphite–tin composites appear to be a good candidates as anodes for lithium-ion batteries.

## References

- [1] H. Oman, MRS Bull. (1999) 33–39.
- [2] A. Manthiram, JOM (1997) 43–46.
- [3] J.B. Goodenough, A. Manthiram, B. Wnetrzewski, J. Power Sources 43/44 (1993) 269–275.
- [4] H. Katz, W. Bögel, J.-P. Büchel, J. Power Sources 72 (1998) 43–50.
- [5] I. Kurabayashi, M. Yokoyama, M. Yamashita, J. Power Sources 54 (1995) 1–5.
- [6] T. Ohzuku, Y. Iwakoshi, K. Sawai, J. Electrochem. Soc. 140 (1993) 2490.
- [7] N. Takami, A. Satoh, M. Hara, T. Ohsaki, J. Electrochem. Soc. 142 (1995) 2564–2571.
- [8] A. Claye, J.E. Fisher, Electrochim. Acta 45 (1999) 107–120.
- [9] K. Sato, M. Noguchi, A. Demachi, N. Oki, M. Endo, Science 264 (1994) 556–558.
- [10] J.R. Dahn, T. Zheng, Y. Liu, J.S. Xue, Science 270 (1995) 590–593.
- [11] T. Zheng, Y. Liu, E.W. Fuller, S. Tseng, U. Von Sacken, J.R. Dahn, J. Electrochem. Soc. 142 (1995) 2581.
- [12] Y.-S. Han, J.-S. Yu, G.-S. Park, J.-Y. Lee, J. Electrochem. Soc. 146 (1999) 3999–4004.
- [13] Y. Idota, T. Kubota, A. Matsufuji, Y. Maekawa, T. Miyasaka, Science 276 (1997) 1395.
- [14] J.O. Besenhard, J. Yang, M. Winter, J. Power Sources 68 (1997) 87–90.
- [15] M.M. Thackeray, J.T. Vaughey, A.J. Kahaian, K.D. Kepler, R. Benedek, Electrochim. Commun. 1 (1999) 111–115.
- [16] O. Mao, R.L. Turner, I.A. Courtney, B.D. Fredericksen, M.I. Buckett, L.J. Krause, J.R. Dahn, Electrochim. Solid State Lett. 2 (1999) 3–5.
- [17] T.D. Shen, W.Q. Ge, K.Y. Wang, M.X. Quan, J.T. Wang, W.D. Wei, C.C. Koch, Nanostruct. Mater. 7 (1996) 393.
- [18] J.B. Aladekomo, R.H. Bragg, Carbon 28 (1990) 897.
- [19] C.S. Wang, G.T. Wu, X.B. Zhang, Z.F. Qi, W.Z. Li, J. Electrochem. Soc. 145 (1998) 2751–2758.
- [20] F. Salver-Disma, C. Lenain, B. Beaudoin, L. Aymard, J.-M. Tarascon, Solid State Ionics 98 (1997) 145–158.
- [21] A. Mabuchi, K. Tokumitsu, H. Fujimoto, T. Kasuh, J. Electrochem. Soc. 142 (1995) 1041.
- [22] K. Tokumitsu, A. Mabuchi, H. Fujimoto, T. Kasuh, J. Electrochem. Soc. 143 (1996) 2235.
- [23] M. Inaba, H. Yoshido, Z. Ogumi, J. Electrochem. Soc. 143 (1996) 2572.
- [24] C.S. Wang, G.T. Wu, W.Z. Li, J. Power Sources 76 (1998) 1–10.